

CrystEngComm

Accepted Manuscript



This is an *Accepted Manuscript*, which has been through the Royal Society of Chemistry peer review process and has been accepted for publication.

Accepted Manuscripts are published online shortly after acceptance, before technical editing, formatting and proof reading. Using this free service, authors can make their results available to the community, in citable form, before we publish the edited article. We will replace this *Accepted Manuscript* with the edited and formatted *Advance Article* as soon as it is available.

You can find more information about *Accepted Manuscripts* in the [Information for Authors](#).

Please note that technical editing may introduce minor changes to the text and/or graphics, which may alter content. The journal's standard [Terms & Conditions](#) and the [Ethical guidelines](#) still apply. In no event shall the Royal Society of Chemistry be held responsible for any errors or omissions in this *Accepted Manuscript* or any consequences arising from the use of any information it contains.

ARTICLE

Crystal growth and magnetic orderings of $\text{Na}_2\text{Ni}_2\text{TeO}_6$ with honeycomb layers and $\text{Na}_2\text{Cu}_2\text{TeO}_6$ with Cu spin dimers

Cite this: DOI: 10.1039/x0xx00000x

Received 00th January 2012,
Accepted 00th January 2012

DOI: 10.1039/x0xx00000x

www.rsc.org/

R. Sankar,^a I. Panneer Muthuselvam,^a G. J. Shu,^a W. T. Chen,^a Sunil K. Karna,^a
R. Jayavel,^b and F. C. Chou,^{*acd}

We report on the crystal growth and magnetic property studies of layered $\text{Na}_2\text{Ni}_2\text{TeO}_6$ and $\text{Na}_2\text{Cu}_2\text{TeO}_6$, the former has a honeycomb layer composed of NiO_6 octahedra and the latter is composed of paired CuO_4 plaquettes connected through TeO_6 octahedron. The 3D antiferromagnetic (AF) phase transition is defined with the peak of $d\chi/dT$ at $\sim 27\text{K}$ for $\text{Na}_2\text{Ni}_2\text{TeO}_6$ and confirmed with specific heat measurement. A comparison is made between the magnetic behavior of $\text{Na}_2\text{Ni}_2\text{TeO}_6$ and $\text{BaNi}_2\text{V}_2\text{O}_8$ with similar Ni-honeycomb network of different centers. $\text{Na}_2\text{Cu}_2\text{TeO}_6$ has been confirmed to have a spin gap of $\Delta/k_B \sim 262\text{K}$ due to spin dimerization of $\text{Cu}^{2+} S=1/2$ within each paired CuO_4 plaquettes..

Introduction

Layered P2-type Na_xCoO_2 has been extensively studied owing its potential for thermoelectric application,¹ similar crystal structure and electrochemical behavior to the battery electrode material Li_xCoO_2 ,² and the peculiar nature of Curie-Weiss metal with superconductivity found when Na content is deintercalated to $x \sim 1/3$ after hydration.³ Variations of P2- Na_xCoO_2 have been tested on $\text{Na}_{2/3}\text{Co}_{2/3}\text{Te}_{1/3}\text{O}_2$ to explore the impact of in-plane (Co/Te) O_2 ordering.⁴ Such in-plane 1/3 substitution to the transition metal elements introduced a novel in-plane honeycomb sublattice, which is expected to show drastically different properties from the original compound of CoO_2 layer in triangular lattice. Additional transition metal substitution with stoichiometric Na content, such as $\text{Na}_2\text{M}_2\text{TeO}_6$ (M= Ni, Zn, Mg), can be prepared and maintained the honeycomb lattice, except for the Cu substitution.⁵

$\text{Na}_2\text{Ni}_2\text{TeO}_6$ can be described as Na layer sandwiched between (Ni/Te) O_6 layers composed of edge-shared NiO_6 and TeO_6 octahedra with symmetry in space group $P6_3/mcm$, similar to the layered Na_xCoO_2 with symmetry in space group $P6_3/mmc$.⁶ The TeO_6 octahedron sits in the center of each honeycomb unit composed of NiO_6 . Preliminary studies of $\text{Na}_2\text{Ni}_2\text{TeO}_6$ using poly crystalline sample suggested that the observed reduction of average spin susceptibilities below $\sim 34\text{K}$ to be an antiferromagnetic transition.⁷ The magnetism of 2D honeycomb lattice is one interesting topic in view of its unique geometry among spins in close relationship to that of the frustrating Kagome and triangular lattices.⁸ The Kosterlitz-

Thouless transition of vortex-antivortex pairing in 2D XY-mode has been one phenomenon expected to be found in the system of 2D honeycomb lattice.⁹ The actual magnetic ordering of spins in honeycomb lattice should be explored in detail using single crystal samples to decouple the crystal and magnetic structures.

Common honeycomb lattice has been found in the layered materials such as $\text{Na}_2\text{M}_2\text{TeO}_6$ (M= Co, Ni, Zn, Mg),⁵⁻⁷ but $\text{Na}_2\text{Cu}_2\text{TeO}_6$ of the similar chemical formula does not show 2D honeycomb lattice, the Cu_2TeO_6 layer is composed of pairs of CuO_4 plaquettes connected with TeO_6 octahedra instead.^{10,11} The reason why $\text{Na}_2\text{Cu}_2\text{TeO}_6$ does not show honeycomb layer symmetry deserves further exploration. Here we report on the successful growth of single crystal samples of both $\text{Na}_2\text{Ni}_2\text{TeO}_6$ and $\text{Na}_2\text{Cu}_2\text{TeO}_6$ samples first time. A full characterization of the crystal structure and the anisotropic spin susceptibilities were performed using the as-grown single crystals.

Experimental section

Material synthesis and crystal growth

Single phase polycrystalline samples of $\text{Na}_2\text{Ni}_2\text{TeO}_6$ and $\text{Na}_2\text{Cu}_2\text{TeO}_6$ were prepared by conventional solid state reaction method. The stoichiometric proportions of high purity Na_2CO_3 , NiO , CuO , and TeO_2 powders were thoroughly mixed and pressed into pellets. These pellets were placed in a platinum crucible and heated to 400°C in air, held for 24 hours and then cooled to room temperature. The pretreated pellets were well ground and pressed into pellets to sinter at 800°C for 24 hours

with slow heating and cooling rates. To obtain single phases, several intermittent grindings and refiring were essentials. The structure and phase purity of the sample were confirmed by powder X-ray diffraction using the synchrotron radiation in NSRRC Taiwan at room temperature, as shown in Fig. 3.

Single crystals of $\text{Na}_2\text{Ni}_2\text{TeO}_6$ and $\text{Na}_2\text{Cu}_2\text{TeO}_6$ were grown using a self flux method. The mixture of pure polycrystalline sample $\text{Na}_2\text{M}_2\text{TeO}_6$ ($\text{M} = \text{Ni}, \text{Cu}$) and the flux of Na_2O and TeO_2 in molar ratio of 1:0.5:2.5 were placed into a platinum crucible, each having mass $\text{Na}_2\text{M}_2\text{TeO}_6$ (30g), Na_2O (10g) and TeO_2 (50g). The crucible was gradually heated to 800°C in air for 30 hours, and then cooled slowly to 500°C at the rate of 2°C h^{-1} , followed by rapid cooling to room temperature. The yields of the obtained crystals turned out to be 70%. The crucible was gradually heated to 800°C in air, held for 30 hours, and then cooled slowly to 500°C at the rate of 2°C h^{-1} , followed by rapid cooling to room temperature. Flaky crystals of $\text{Na}_2\text{M}_2\text{TeO}_6$ ($\text{M} = \text{Ni}$ and Cu) with typical size of 3-8 mm in diameter and ~ 0.5 mm thick in light green color for $\text{Na}_2\text{Ni}_2\text{TeO}_6$ and dark green color for $\text{Na}_2\text{Cu}_2\text{TeO}_6$ were obtained at the top of the crucible. The excessive selfflux can be washed off with hot 1M NaOH solution.

Crystal structure analysis and magnetization measurement Initial phase characterization was carried out using lab X-ray diffractometer and further crystal structure analysis was conducted with synchrotron X-ray powder diffraction (SXRD). The SXRD pattern was collected at room temperature with crushed crystal at beamline in National Synchrotron Radiation Research Center (NSRRC), Taiwan with 20 keV energy which corresponds to wavelength of 0.619925 \AA . The obtained patterns were analyzed with the Rietveld method using the General Structure Analysis System (GSAS) software package. All diffraction peaks of $\text{Na}_2\text{Ni}_2\text{TeO}_6$ and $\text{Na}_2\text{Cu}_2\text{TeO}_6$ can be indexed with hexagonal $\text{P6}_3/\text{mcm}$ symmetry and monoclinic C2/m , respectively, as shown in Fig. 3 and Tables 1 and 2, in agreement with the previous reports.⁷⁻¹⁰

Figure 3 displays the observed and fitted x-ray diffraction patterns of the $\text{Na}_2\text{Ni}_2\text{TeO}_6$ and $\text{Na}_2\text{Cu}_2\text{TeO}_6$ at 300K, with their differences plotted at the bottom. The observed and fitted patterns agree very well, with a profile R-factor of $R_p = 3.92\%$, a weighted profile R-factor of $R_{wp} = 4.88\%$, and a goodness factor of $\chi^2 = 3.854$. All sites are fully occupied giving rise to chemical compositions of $\text{Na}_2\text{Ni}_2\text{TeO}_6$ and $\text{Na}_2\text{Cu}_2\text{TeO}_6$. In addition, elemental analysis using EMPA taken from 10 different portions of the sample gives an atomic ratio of $\text{Na}:\text{Ni}:\text{Te}=39.32:40.38:20.30$ and $\text{Na}:\text{Cu}:\text{Te}=39.77:39.87:20.36$ close to the presumed stoichiometry. Reflection Laue patterns (insets of Fig. 3) of the as grown single crystals confirm the crystallinity of both $\text{Na}_2\text{Ni}_2\text{TeO}_6$ and $\text{Na}_2\text{Cu}_2\text{TeO}_6$.

SQUID magnetometer was employed to measure the homogeneous spin susceptibility (M/H) as a function of temperature in the range of 2-300K under applied fields of 100 Oe and 1 Tesla, for both polycrystalline (crushed crystals) and single crystal samples. The magnetic field is applied along and perpendicular to the honeycomb lattice plane. Heat capacity

was measured with a standard relaxation method (PPMS, Quantum Design).

Results and discussions

Crystal Structure

The $\text{Na}_2\text{Ni}_2\text{TeO}_6$ crystallizes into hexagonal $\text{P6}_3/\text{mcm}$ symmetry, where Na atoms could locate at three different crystallographic sites in the layer with occupancies expected adding up to 1. The total Na content is not expected to be stoichiometric for powder samples prepared in the air and at high temperatures.⁵ Comparing to Na_xCoO_2 prepared in the air under ambient pressure, Na vacancy could lead to vacancy superlattice orderings.¹² Preliminary study of $\text{Na}_2\text{Ni}_2\text{TeO}_6$ powder sample with Na content adjustment does show signature of two phases with slightly different onsets of magnetic orderings near 25-30K. However, the single crystal samples grown using $\text{Na}_2\text{O} + \text{TeO}_2$ flux show Na content to be close to stoichiometry within error of 0.01, as confirmed by both electron probe microanalysis (EPMA) and inductively coupled plasma (ICP) analysis.

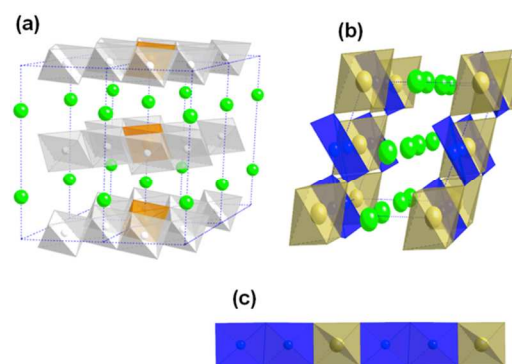


Fig.1 Crystal structures of (a) $\text{Na}_2\text{Ni}_2\text{TeO}_6$ with honeycomb lattice composed of NiO_6 octahedra. There are three different crystallographic sites of various occupancies for Na but only the Na3 sites are shown. (b) Crystal structure of $\text{Na}_2\text{Cu}_2\text{TeO}_6$ with (c) paired CuO_4 plaquettes which are connected through TeO_6 octahedra.

The crystal structure of $\text{Na}_2\text{Ni}_2\text{TeO}_6$ (Fig. 1) can be viewed as a honeycomb lattice composed of edge-shared NiO_6 octahedra, as shown in Fig. 2(a). Comparing to $\text{BaNi}_2\text{V}_2\text{O}_8$, a compound with similar honeycomb lattice composed of NiO_6 edge-sharing octahedra, $\text{BaNi}_2\text{V}_2\text{O}_8$ consists of two triangular pyramidal VO_4 units in the honeycomb center,¹³ in contrast to $\text{Na}_2\text{Ni}_2\text{TeO}_6$ with TeO_6 octahedron sitting in the honeycomb center.

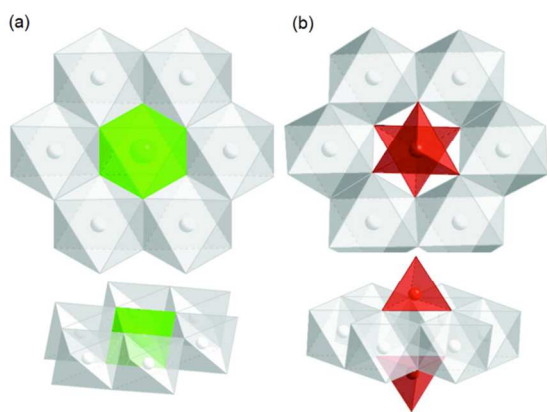


Fig. 2 The honeycomb lattices of $\text{Na}_2\text{Ni}_2\text{TeO}_6$ and $\text{BaNi}_2\text{V}_2\text{O}_8$ composed of NiO_6 with TeO_6 octahedron and VO_4 double trigonal pyramids sitting in the honeycomb center, respectively.

Although $\text{Na}_2\text{Cu}_2\text{TeO}_6$ exhibits similar chemical formula to that of $\text{Na}_2\text{Ni}_2\text{TeO}_6$, it is interesting to observe that the former does not form a similar 2D honeycomb lattice. $\text{Na}_2\text{Cu}_2\text{TeO}_6$ can be viewed as a layered compound having Na ions sandwiched between the effective planes of Cu_2TeO_6 ^{10, 11}. The main reason behind the absence of honeycomb lattice in $\text{Na}_2\text{Cu}_2\text{TeO}_6$ lies on the preferable CuO_4 plaquette coordination, which has been demonstrated repeatedly in many layered transition metal oxides, such as cuprate superconductors with Cu-O chain, ladder, or planes.¹⁴

We also noted that another chemically similar compound of $\text{Li}_2\text{Ni}_2\text{TeO}_6$ with identical layered structure of $\text{Na}_2\text{Ni}_2\text{TeO}_6$ can be prepared through a topochemical route through ion exchange,¹⁵ In addition, direct high temperature reaction for $\text{Li}_2\text{Ni}_2\text{TeO}_6$ preparation led to an orthorhombic structure of $Fddd$ symmetry with disordered Li/Ni. A complete single crystal study for layered $\text{Na}_2\text{Ni}_2\text{TeO}_6$, orthorhombic $\text{Li}_2\text{Ni}_2\text{TeO}_6$, and topochemically prepared $\text{Li}_2\text{Ni}_2\text{TeO}_6$ has been proposed and under way.

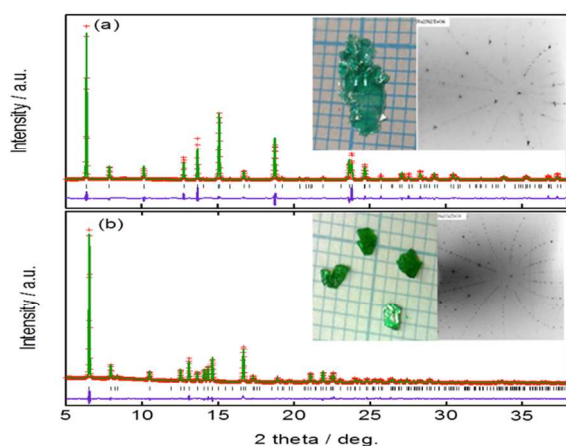


Fig. 3 Synchrotron X-ray powder diffraction patterns and the results of Rietveld refinement of (a) $\text{Na}_2\text{Ni}_2\text{TeO}_6$ and (b) $\text{Na}_2\text{Cu}_2\text{TeO}_6$. The observed pattern, calculated profile, and the Bragg peak positions are shown with cross marks, a green curve, and tick marks, respectively.

The bottom curve shows the difference between the observed and calculated intensities. The crystal photos and the corresponding Laue patterns of the as-grown crystals are shown in the insets.

2D to 3D phase transition in $\text{Na}_2\text{Ni}_2\text{TeO}_6$

The anisotropic behavior of average spin susceptibilities (M/H) as a function of temperature for $\text{Na}_2\text{Ni}_2\text{TeO}_6$ is shown in Fig. 4. The high temperature region exhibits Curie-Weiss behaviour and an antiferromagnetic (AF) like broad peak is observed near ~ 30 K. The Curie-Weiss law fitting ($\chi(T) = \chi_0 + C/(T - \theta)$) for the powder average data indicates that $C = 2.968(1) \text{ cm}^3\text{-K/mole}$ and $\theta = -32\text{K}$, which suggests that Ni ion has an effective moment of $3.446 \mu_B$. Since $3d^8$ of Ni^{2+} with octahedral crystal field e_g-t_{2g} splitting must have electronic configuration as $e_g^2 t_{2g}^6$ of $S=1$, $\mu_{\text{eff}} = 2.828 \mu_B$ is expected for $S=1$ (assuming $g=2$) from spin-only contribution. The experimental value of $\mu_{\text{eff}} = 3.446 \mu_B$ per Ni^{2+} is larger than that predicted by the spin-only value for $S=1$, which has often been suggested due to orbital contribution represented as an effective g -factor larger than 2.⁷

The magnetic susceptibility at low temperatures (Fig. 4) shows that the anisotropic behaviour of $\text{Na}_2\text{Ni}_2\text{TeO}_6$ has a typical antiferromagnetic ordering with spins aligned along the c -axis. Although it is tempting to assign the peak near 30K to be the onset of a 3D AF long range ordering (LRO),⁷ however, the transition has a $\chi(T)$ peak width smoother than that expected from a transition of 3D AF LRO, which strongly suggests that the broad peak near 30K is resulted from a 2D AF short range ordering (SRO), i.e., the inter-layer correlation length must develop long enough to reach the 3D LRO below 30K. Similar broad SRO behavior has been observed in $\text{BaNi}_2\text{V}_2\text{O}_8$ of a similar honeycomb lattice composed of NiO_6 octahedra.¹³ 3D AF ordering of Ni within and between honeycomb lattice of $\text{BaNi}_2\text{V}_2\text{O}_8$ has been found consistent to the expected magnetic neutron diffraction pattern,^{7, 13} although $\text{BaNi}_2\text{V}_2\text{O}_8$ has a much broader range of 2D SRO evolution without a clear 3D onset of AF LRO.¹³ $\text{Na}_2\text{Ni}_2\text{TeO}_6$ has a round peak of 2D SRO character as shown in $\chi(T)$ near 30K, in particular, there exists a steep drop of $\chi(T)$ below $\sim 30\text{K}$ to be only revealed by the peak of its derivative ($d\chi/dT$) near $\sim 27\text{K}$ (Fig. 5). Based on current anisotropic spin susceptibility measurement results shown in Fig. 4, the AF ordering for $\text{Na}_2\text{Ni}_2\text{TeO}_6$ has an easy axis along the c -direction that is perpendicular to the honeycomb lattice plane. Since the in-plane Ni-Ni distance of $\text{Na}_2\text{Ni}_2\text{TeO}_6$ (3.00 \AA) is longer than that of $\text{BaNi}_2\text{V}_2\text{O}_8$ (2.905 \AA),^{5, 13} it is feasible to find that $\text{Na}_2\text{Ni}_2\text{TeO}_6$ has lower onsets of 2D and 3D ordering temperature as a result of the weaker nearest neighbor Ni-Ni coupling strength. Structurally, the shorter Ni-Ni distance for $\text{BaNi}_2\text{V}_2\text{O}_8$ could be due to the stronger corner sharing double VO_4 trigonal pyramid sitting in the middle of NiO_6 honeycomb unit of $\text{BaNi}_2\text{V}_2\text{O}_8$ (Fig. 2). On the other hand, Tellurium (Te) having larger atomic size is filled up to $n=5$, a larger TeO_6 sitting in the middle of NiO_6 honeycomb network leads to longer Ni-Ni distance and results in the weakening of Ni-Ni coupling as expected.

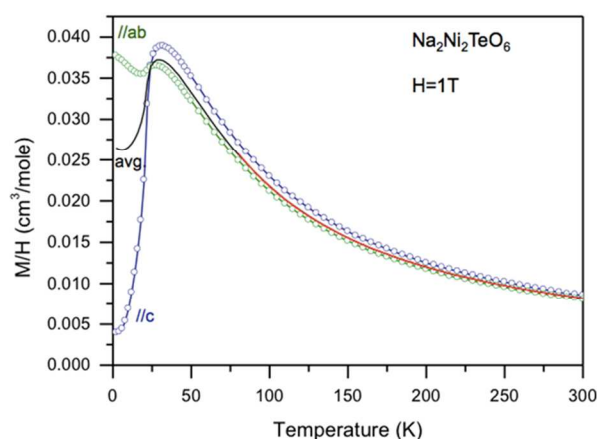


Fig. 4 Homogeneous spin susceptibilities (M/H) of $\text{Na}_2\text{Ni}_2\text{TeO}_6$ for $H=1$ Tesla applied perpendicular and parallel to the c -axis. Powder average is shown in black solid line, and the red solid line represents the Curie-Weiss and HTSE fittings.

The powder averaged $d\chi(T)/dT$ data is shown in Fig. 5, which reveals a sharp drop of $\chi(T)$ of 3D AF character below the 2D SRO regime to signify the onset of a 3D AF LRO. We have performed specific heat measurement in the same temperature range. The peaks of C_p and $d\chi(T)/dT$ coincide at $\sim 27\text{K}$, which suggests that the actual 3D T_N should be defined at $\sim 27\text{K}$, instead of the broad peak near 30K .⁷ A similar broad feature of $d\chi/dT$ has been found below T_N in $\text{Na}_2\text{Co}_2\text{TeO}_6$, which was tentatively assigned to spin reorientation due to unknown origin.⁴ Kosterlitz and Thouless (KT) have proposed the existence of a topological phase transition caused by the vortex-antivortex pairing within 2D XY system, which could be viewed as a quasi-ordered phase with nonzero correlation function decreases with distance.¹⁶ KT transition has been suggested to be a compatible interpretation for $\text{BaNi}_2\text{V}_2\text{O}_8$ as a weak anisotropic 2D Heisenberg antiferromagnet.⁹ However, current $d\chi/dT$ data of $\text{Na}_2\text{Ni}_2\text{TeO}_6$ do not provide enough evident to indicate the existence of a KT transition, a clear 3D AF LRO has been suggested based on the agreement of $d\chi/dT$ and C_p results. In addition, the Na in-plane disordering (three crystallographic sites of unequal occupancies) and the potential oxygen vacancies could complicate the search of KT transition in $\text{Na}_2\text{Ni}_2\text{TeO}_6$, in comparing to the $\text{BaNi}_2\text{V}_2\text{O}_8$ with ordered Ba layer.

The magnetic part of the heat capacity C_{mag} for $\text{Na}_2\text{Ni}_2\text{TeO}_6$ is obtained by subtracting the C_p of $\text{Na}_2\text{Zn}_2\text{TeO}_6$ from the total, because the latter is an isostructural analogue of $\text{Na}_2\text{Ni}_2\text{TeO}_6$ without magnetic contribution. The magnetic entropy, S_{mag} , was deduced from the temperature integration of C_{mag} through $S_{\text{mag}} = \int C_{\text{mag}}/T dT$. As seen in the inset of Fig.5, S_{mag} of $\text{Na}_2\text{Ni}_2\text{TeO}_6$ is saturated to $\sim 16.44 \text{ J/mol K}$ near 120K , which is about 90% of the theoretical magnetic entropy of $S_{\text{mag}} = 2R\ln(2S+1) \sim 18.27 \text{ J/mol K}$. On the other hand, the entropy gain from the 3D LRO below T_N is about 1/3 of the total S_m , which suggests that significant amount of entropy is gained above T_N to reflect a reduced dimensionality.

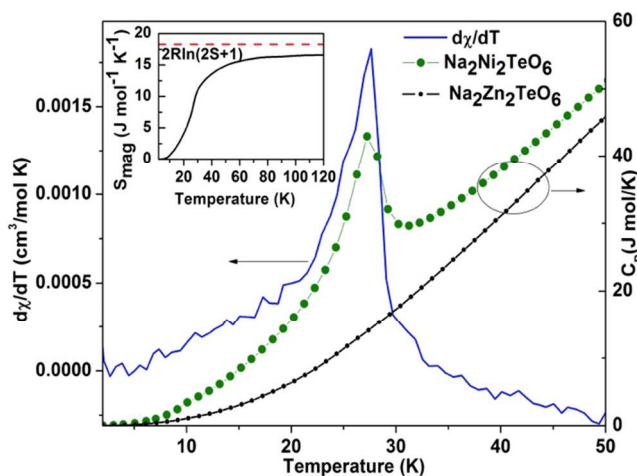


Fig.5 Specific heat of $\text{Na}_2\text{Ni}_2\text{TeO}_6$ shows the exothermic peak coincides with the peak of $d\chi/dT$ (T) derived from Fig. 4, which suggests the actual 3D AF LRO onset is near 27K , instead of the round peak which represents 2D SRO near $\sim 30\text{K}$. The inset shows an estimate of magnetic entropy for $\text{Na}_2\text{Ni}_2\text{TeO}_6$.

Magnetic moment of Ni in $\text{Na}_2\text{Ni}_2\text{TeO}_6$

Based on the Curie-Weiss law fitting, the measured μ_{eff} ($=3.446\mu_B$) is significantly larger than that of the expected spin-only value of $2.828\mu_B$ ($g=2$) for $S=1$, which has often been described due to spin-orbital coupling as $g > 2$ without a clear physical picture.⁷ The assumed ionic charge balance of $\text{Na}^+\text{Ni}^{2+}_2\text{Te}^{6+}\text{O}^{2-}_6$ suggests that the $\mu_{\text{eff}} = 3.446\mu_B$ corresponds to Ni^{2+} at $S=1$ with an effective g -factor of 2.437. In fact, $\text{Na}_2\text{Ni}_2\text{TeO}_6$ could have two possible arrangements of charge under the extreme ionic model as $\text{Na}^{1+}_2\text{Ni}^{2+}_2\text{Te}^{6+}\text{O}^{2-}_6$ or $\text{Na}^{1+}_2\text{Ni}^{3+}_2\text{Te}^{4+}\text{O}^{2-}_6$. We have tested these two hypotheses using bond valence sum (BVS) method with the synchrotron XRD results. BVS analysis using $\text{Ni}^{2+}/\text{Te}^{6+}$ parameters suggests that valences for Ni and Te cations are close to 2.33 and 5.04, respectively. When $\text{Ni}^{3+}/\text{Te}^{4+}$ parameters were used, the resultant valences for Ni and Te cations are close to 2.85 and 5.58, respectively. Clearly both BVS results are not satisfactory, which indicates the possibility of an intermediate state. In contrast, BVS analysis for $\text{Na}_2\text{Cu}_2\text{TeO}_6$ shows that the valences of 2.05 and 5.57 for Cu and Te agree satisfactorily with the assumption of $\text{Cu}^{2+}/\text{Te}^{6+}$, which indirectly supports the unconventional charge balance between Ni and Te in $\text{Na}_2\text{Ni}_2\text{TeO}_6$. A separate neutron diffraction experiment has been proposed to tackle this problem more effectively. In addition to the Curie-Weiss law fitting, high temperature series expansion (HTSE) fitting results for $\text{Na}_2\text{Ni}_2\text{TeO}_6$ are also shown in Fig. 4 with best fitting of $C=2.919(1) \text{ cm}^3/\text{mole}$ and $J/k_B=45.3(1)\text{K}$ up to the third order. The nearest neighbor coupling J implies that the T_N of 3D LRO follows the relationship of $T_N = \alpha J/k_B$ with $\alpha \sim 0.6$, which is in agreement to the AF transition for most layered compounds moving from 2D to 3D.¹⁷

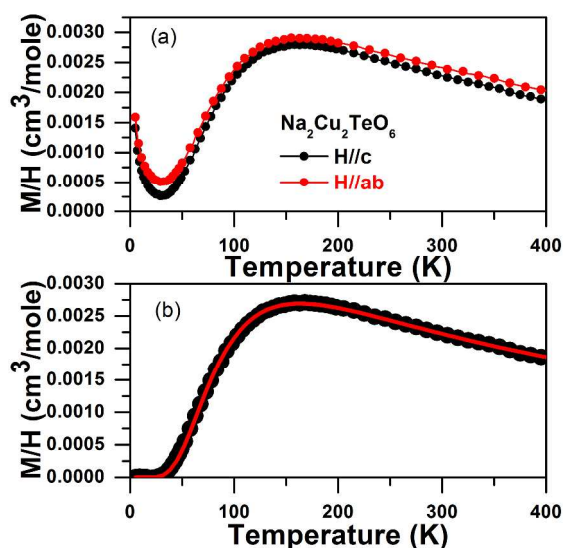


Fig. 6 (a) The magnetic susceptibilities of $\text{Na}_2\text{Cu}_2\text{TeO}_6$ measured with applied field applied in orientations perpendicular and parallel to the honeycomb planes. (b) The powder averaged magnetic spin susceptibilities of $\text{Na}_2\text{Cu}_2\text{TeO}_6$ after impurity Curie contribution. The data are fitted with Bleaney-Bowers equation for the isolated dimers of spin gap $\Delta/k_B \sim 262\text{K}$ and inter-dimer coupling $J/k_B \sim 209\text{K}$.

Spin-dimerization of $\text{Na}_2\text{Cu}_2\text{TeO}_6$

Fig. 6 displays the temperature dependence of the powder averaged and anisotropic magnetic susceptibilities for $\text{Na}_2\text{Cu}_2\text{TeO}_6$ single crystal sample. After the subtraction of a small paramagnetic contribution from the impurity spins with Curie's law fitting at low temperatures from the powder averaged data, a spin gap is revealed clearly for $T \rightarrow 0\text{K}$, which is consistent to a spin gap opening with $\Delta/k_B \sim 205(3)\text{K}$ following the fitting of $\chi = \chi_0 + A \exp(-\Delta/k_B T)$ at low T , by assuming an activation behavior of a two level system with a singlet ground state.¹⁷ Based on the crystal structure of edge-shared CuO_4 pair plaquettes that are connected by the nonmagnetic TeO_6 octahedra within each Cu_2TeO_6 layer, as shown in Fig. 1(b)-(c), it is reasonable to assume that the spin gap opening results from a spin dimerization of $\text{Cu}^{2+} S=1/2$ within each pair of edge-shared CuO_4 plaquettes.

For powder averaged $\chi(T)$ data after the subtraction of PM contribution from the impurities or defects, the best fit using the Bleaney-Bowers equation for $S=1/2$ dimers of spin gap Δ with interdimer coupling J gives $g=2.39(1)$, $J/k_B = 209(11)\text{K}$, and $\Delta/k_B = 261.6(4)\text{K}$, which are consistent to the observed spin susceptibility with a spin gap describable from the activation behavior of a two level system.^{18,19} These results are also in agreement with that reported by Morimoto et al. using both uniform spin susceptibility and NMR measurements.¹¹ The inter-dimer coupling J is comparable to the gap size and obviously not negligible for the dimerized system, which has been reflected on the crystal structure where Cu dimers within spin chain along the b-direction are coupled through the Cu-O-Te-O-Cu super-super

exchange route between the paired CuO_4 plaquettes and the TeO_6 octahedra, as shown in Fig. 1(b)-(c).

Conclusions

In summary, we have reported the growth recipe first time and magnetic properties of $\text{Na}_2\text{Ni}_2\text{TeO}_6$ and $\text{Na}_2\text{Cu}_2\text{TeO}_6$ single crystals. $\text{Na}_2\text{Ni}_2\text{TeO}_6$ has a honeycomb lattice composed of NiO_6 octahedra and spin orders in short range near $\sim 30\text{K}$ before 3D AF ordering is achieved below $T_N \sim 27\text{K}$. On the other hand, the $\text{Na}_2\text{Cu}_2\text{TeO}_6$ with a Cu_2TeO_6 layer containing edge-shared CuO_4 plaquettes has shown spin gap opening as a result of spin dimerization.

Acknowledgements

FCC acknowledges the support provided by the Ministry of Science and Technology of Taiwan under project number NSC-102-2119-M-002-004..

Notes

^a Center for Condensed Matter Sciences, National Taiwan University, Taipei 10617, Taiwan.

^b Anna University, Crystal Growth Centre, Chennai-600025, India,

^c National Synchrotron Radiation Research Center, Hsinchu 30076, Taiwan,

^d Taiwan Consortium of Emergent Crystalline Materials, National Science Council, Taipei 10622, Taiwan

E-mail: fcchou@ntu.edu.tw, sankarndf@gmail.com

References

- (1) I. Terasaki, *J. Appl. Phys.*, 2011, **110**, 053705.
- (2) J. T. Hertz, Q. Huang, T. McQueen, T. Klimczuk, J. W. G. Bos, L. Viciu, and R. J. Cava, *Phys. Rev B*, 2008, **77**, 075119.
- (3) K. Takada, H. Sakurai, E. Takayama-Muromachi, F. Izumi, R. A. Dilanian, and T. Sasaki, *Nature*, 2003, **422**, 53.
- (4) L. Viciu, Q. Huang, E. Morosan, H. W. Zandbergen, N. I. Greenbaum, T. McQueen, and R. J. Cava, *J. Solid State Chem.* 2007, **180**, 1060.
- (5) M. A. Evstigneeva, V. B. Nalbandyan, A. A. Petrenko, B. S. Medvedev, and A. A. Kataev, *Chem. Mater.*, 2011, **23**, 1174.
- (6) F.-T. Huang, M.-W. Chu, G. J. Shu, H. Sheu, C. Chen, L.-K. Liu, P. Lee, and F. C. Chou, *Phys. Rev. B*, 2009, **79**, 014413.
- (7) R. Berthelot, W. Schmidt, A. W. Sleight, and M. A. Subramanian, *J. Solid State Chem.*, 2012, **196**, 225.
- (8) J. S. Gardner, M. J. P. Gingras, and J. E. Greedan, *Rev. Mod. Phys.* 2010, **82**, 53.
- (9) M. Heinrich, H.-A. Krug Von Nidda, A. Loidl, N. Rogado, and R. J. Cava, *Phys. Rev. Lett.* 2003, **91**, 137601.
- (10) J. Xu, A. Assoud, N. Soheilnia, S. Derakhshan, H. L. Cuthbert, J. E. Greedan, M. H. Whangbo, and H. Kleinke, *Inorg. Chem.* 2005, **44**, 5042.
- (11) K. Morimoto, Y. Itoh, K. Yoshimura, M. Kato, and K. Hirota, *J. Phys. Soc. Jpn.* 2006, **75**, 083709.

- (12) G. J. Shu, A. Prodi, S. Y. Chu, Y. S. Lee, H. S. Sheu, and F. C. Chou, *Phys. Rev. B* 2007, **76**, 184115.
- (13) N. Rogado, Q. Huang, J. Lynn, A. Ramirez, D. Huse, and R. J. Cava, *Phys. Rev. B* 2002, **65**, 144443.
- (14) T. Timusk and B. Statt, *Rep. Prog. Phys.* 1999, **62**, 61.
- (15) Vinod Kumar, Akanksha Gupta, S. Uma, Dalton Transactions 2013, **42(42)**, 14992-14998
- (16) J. M. Kosterlitz and D. J. Thouless, *J. Phys C: Solid State Physics*, 2002, **6**, 1181.
- (17) D. Johnston, R. Kremer, M. Troyer, X. Wang, A. Klumper, S. Bud'ko, A. Panchula, and P. Canfield, *Phys. Rev. B* 2000, **61**, 9558.
- (18) T. Nakajima, H. Mitamura, and Y. Ueda, *J. Phys. Soc. Jpn.*, 2006, **75**, 054706.
- (19) B. Bleaney and K. D. Bowers, *Proc. R. Soc. London, Ser. A* 1952, **214**, 451.

Table 1 Structure parameters derived from the Rietveld refinements of $\text{Na}_2\text{Ni}_2\text{TeO}_6$ at room temperature with space groups $P6_3/mcm$. $a=b=5.1988(1)$ Å, $c=11.1277(4)$ Å, $\chi^2=6.29$. (* The Isotropic thermal parameter U_{iso} of oxygen was constrained to be identical by atom type).

Atom	Site	x	y	z	* $U_{\text{iso}}/\text{Å}^2$
Te	2b	0	0	0	0.0147(8)
Ni	4d	2/3	1/3	0	0.0049(8)
O	12k	0.673(2)	0.673(2)	0.5917(2)	0.015(2)
Na1	6g	0.339(4)	0	0.25	0.026(6)
Na2	4c	1/3	2/3	0.25	0.026(6)
Na3	2a	0	0	0.25	0.026(6)

Table 2 Structure parameters derived from the Rietveld refinements of $\text{Na}_2\text{Cu}_2\text{TeO}_6$ at room temperature with space groups $C12/m1$. $a=5.6980(1)$ Å, $b=8.6518(2)$ Å, $c=5.9359(1)$ Å, $\alpha=90.059(1)$, $\beta=113.685(1)$, $\gamma=89.914(1)$, $\chi^2=7.44$. (* The Isotropic thermal parameter U_{iso} of oxygen was constrained to be identical by atom type).

Atom	Site	x	y	z	* $U_{\text{iso}}/\text{Å}^2$
Te	2a	0	0	0	0.0153(9)
Cu	4g	0	0.6664(4)	0	0.0148(9)
Na	4h	0	0.180(1)	0.5	0.021(2)
O1	8j	0.197(1)	0.168(2)	0.211(1)	0.009(2)
O2	4i	0.759(2)	0	0.154(2)	0.009(2)